Macromolecular Solute Transport in Supramolecular Hydrogels Spanning Dynamic to Quasi-Static States

Adam S. Braegelman^{1,2}, Rachel C. Ollier¹, Bo Su¹, Christopher J. Addonizio¹, Lei Zou¹, Sara L. Cole³, Matthew J. Webber^{1,*}

- ¹University of Notre Dame, Department of Chemical & Biomolecular Engineering, Notre Dame, IN 46556 USA
- ² University of Notre Dame, Bioengineering PhD Program, Notre Dame, IN 46556 USA
- ³University of Notre Dame, Integrated Imaging Facility, Notre Dame, IN 46556 USA
- *- mwebber@nd.edu

ABSTRACT: Hydrogels prepared from supramolecular crosslinking motifs are appealing for use as biomaterials and drug delivery technologies. The inclusion of macromolecules (e.g., protein therapeutics) in these materials is relevant to many of their intended uses. However, the impact of dynamic network crosslinking on macromolecule diffusion must be better understood. Here, hydrogel networks with identical topology but disparate crosslink dynamics are explored. These materials are prepared from crosslinking with host-guest complexes of the cucurbit[7]uril (CB[7]) macrocycle and two guests of different affinity. Rheology confirms differences in bulk material dynamics arising from differences in crosslink thermodynamics. Fluorescence recovery after photobleaching (FRAP) provides insight into macromolecule diffusion as a function of probe molecular weight and hydrogel network dynamics. Together, both rheology and FRAP enable the estimation of mean network mesh size, which is then related to the solute hydrodynamic diameters to further understand macromolecule diffusion. Interestingly, the thermodynamics of host-guest crosslinking are correlated with a marked deviation from classical diffusion behavior for higher molecular weight probes, yielding solute aggregation in high-affinity networks. These studies offer insights into fundamental macromolecular transport phenomena as it relates to the association dynamics of supramolecular networks. Translation of these materials from in vitro to in vivo is also assessed by bulk release of an encapsulated macromolecule. Contradictory in vitro to in vivo results, with inverse relationships in release between the two hydrogels, underscores the caution demanded when translating supramolecular biomaterials into application.

KEYWORDS: Self-Assembly; Bioinspired Materials; Soft Matter; Materials Chemistry; Injectable Gels

INTRODUCTION

Hydrogels have been routinely explored for a variety of applications in biomedicine.¹⁻³ An ability to imbue aqueous media in amounts many times the mass of their dry material constituents affords a highly hydrated porosity resembling percolated mesh-like structures of the extracellular matrix. Given specific relevance in developing nascent drug delivery systems and synthetic biomaterials, understanding the diffusion behavior of soluble macromolecules through hydrogels is of great interest. This property indeed dictates the types of therapeutic payloads that can be delivered from within a hydrogel, the rate and duration of such release, the infiltration of

physiological entities, and the viability of encapsulated cells. The diffusion of macromolecular solutes within hydrogels has thus been extensively explored, with rich transport phenomena and mathematical models derived on the basis of parameters such as mesh size, crosslink density, chain or crosslink dynamics, and solute hydrodynamic radius.⁴⁻⁶

Supramolecular chemistry is an area of expanding focus in materials design, with many classes of materials being demonstrated to prepare hydrogels for uses in drug delivery and as biomaterials.^{7,8} These materials are typically prepared from molecular-scale recognition motifs that self-assemble to form dynamic physical crosslinks giving rise to network formation.

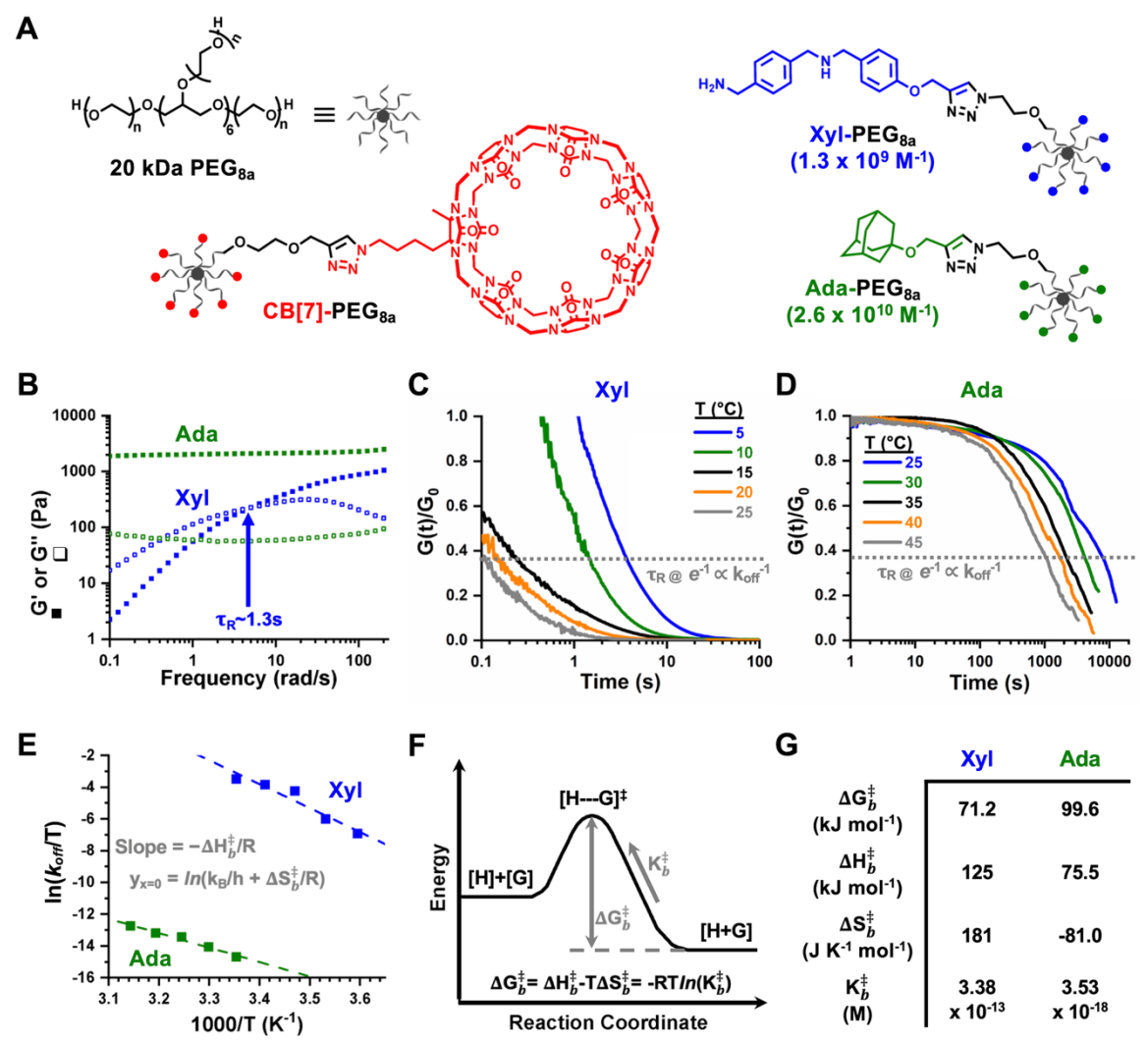


Figure 1. (a) Schematics and molecular structures of 8-arm PEG macromers used to form hydrogels, including the monovalent molecular-scale binding affinities of the various motifs explored. (b) Variable frequency dynamic oscillatory rheology at 2% strain displaying the disparate dynamics of CB[7]–guest hydrogels arising from the affinity of the crosslinking motif used. (c) Stress relaxation by oscillatory rheology at 2% strain of more dynamic Xyl-based hydrogels and (d) less dynamic Ada-based hydrogels at different temperatures. (e) Transition state theory performed *via* Eyring analysis of stress relaxation data at relevant temperatures, wherein k_{off} of each sample is the inverse of τ_R at $G(t)/G_0 = e^{-1}$, R is the gas constant, k_B is the Boltzmann constant, and h is the Planck constant. (f) Energy diagram depicting the thermodynamic parameters arising from Eyring analysis on the transition state for dynamic crosslinks. (g) Table of thermodynamic parameters governing conversion from the bound to transition state (ΔG^{\ddagger}) for Xyl and Ada hydrogels obtained from Eyring analysis.

In particular, these dynamic materials offer mimics of the dynamic nature of living biological materials. Crosslinking on the basis of host–guest recognition provides a reliable means to prepare supramolecular hydrogels for a variety of applications, with the underlying affinity and dynamics of the recognition motif translating to control over bulk hydrogel mechanics. 9–11 Both affinity and dynamics may further be designed and tuned to respond to assorted stimuli relevant for therapeutic use. 12 In addition, host–guest recognition offers specific utility in creating materials that shear-thin and self-heal for injection-centered delivery. 13 One synthetic macrocycle of interest in preparing hydrogels is cucurbit [7] uril (CB[7]), known

for its ability to bind a variety of guest motifs with a wide range of accessible and tunable binding affinities (K_{eq}) . ^{14–16} CB[7] recognition accounts for the highest ever-reported monovalent small molecule binding motif, with Keq values of up to ~1017 M-1 reported.17 As K_{eq} is directly related to the association/disassociation rates of host-guest complexes, CB[7] enables the exploration of crosslinking dynamics over a range unattainable by other commonly available macrocycles. 18,19 Hydrogels prepared via CB[7]-guest crosslinking thus afford a useful model system to study the impact of crosslink dynamics on emergent material properties and functions.

Herein, CB[7]-guest ideal network hydrogels were used in order to understand the impact of crosslink dynamics on the diffusion and release of model macromolecular solutes.18 By mixing 8-arm polyethylene glycol (PEG) macromers terminated with either CB[7] or a complementary guest of tunable affinity, ideal network hydrogels were formed via CB[7]-guest physical crosslinking (Fig 1A). Guest affinities were selected to form stable hydrogels with rheological properties spanning dynamic to quasistatic states. These materials were characterized rheologically to assess thermodynamic complex stability before exploring the impact of crosslink dynamics and macromolecular solute dimensions on diffusion within the networks. Finally, in anticipation of using this class of materials for macromolecular drug delivery, their release properties were explored and compared in vitro and in vivo.

RESULTS & DISCUSSION

Hydrogel Preparation. In this work, two hydrogels of differing crosslink dynamics were prepared and investigated to study the impact of supramolecular dynamics on macromolecular solute crosslink diffusion and release. These studies leveraged previously reported methods for quantitative modification of 8-arm PEG macromers with CB[7] and its guests. 18 Bulk rheological properties were targeted to facilitate dynamics on biologically relevant timescales, an outcome achieved through selection of two distinct guest chemistries for presentation on PEG macromers (Fig 1A). The first hydrogel (Xyl) was prepared by equimolar mixing of CB[7]-PEG8a with a a macromer decorated with terminal complementary p-xylylenediamine guest motifs (Xyl-PEGsa) at a total macromer concentration of 5 wt%. This Xyl guest has a reported molecular-scale affinity for CB[7] of $K_{eq} = 1.3$ x 109 M⁻¹.18 The second hydrogel (Ada) was prepared instead with equimolar addition of a guest-bearing macromer decorated with terminal 1-adamantanol (Ada-PEG8a), also at a total macromer concentration of 5 wt%. This Ada guest has a reported molecular-scale affinity for CB[7] of $K_{eq} = 2.6 \times 10^{10} \text{ M}^{-1}.^{18}$ It is noted that the affinities for both guests were determined on the molecular scale in deionized water by competition ¹H NMR experiments. Host-guest affinity is expected to be reduced upon conjugation onto macromers as a consequence of a reduced rate of association (k_{on}) as well as increased entropic penalty for the association of macromers relative to that for small molecules,

though characterization of such phenomena remains in need of more extensive study.

The affinity of a host–guest interaction is related to its dynamics of association and dissociation as follows:

$$K_{eq} \cong \frac{k_{on}}{k_{off}} \tag{1}$$

where the binding affinity (K_{eq}) is approximated by the ratio of the association rate (k_{on}) to the dissociation rate (k_{off}). It is known for physical crosslinking of hydrogels that network dynamics, and specifically the relaxation time (τ_R), are inversely related to k_{off} ($\tau_R \approx 1/k_{off}$), which can be approximated from the crossover point (ω_c) of the storage modulus (G') and the loss modulus (G'') in a variable frequency oscillatory rheology experiment.²⁰ First, a strain sweep was conducted at 10 rad/s in order to verify the linear viscoelastic region of these materials (Fig S1); from these results, a variable frequency study was performed at 2% strain as this was well within the linear viscoelastic region for both Xyl and Ada hydrogels. Differences in crosslink dynamics were indeed evident in oscillatory rheology, consistent with expectations based on the differences in K_{eq} of the underlying CB[7]–guest interactions. Frequency sweeps (Fig 1B) performed on the Xyl hydrogel featured a G'/G'' crossover of $\omega_c = 4.82$ rad/s, corresponding to $\tau_R \approx 1.3$ s; the Ada hydrogel had sufficiently slow dynamics to not enable an observable point. Instead, Ada demonstrated frequency-independent behavior typically seen for static covalent networks. It is noted that ω_c in the Xyl hydrogel is ~1 order of magnitude higher than was previously reported for this same material.¹⁸ This effect is hypothesized to arise from the present studies being performed in phosphate buffered saline, versus deionized water used previously. It is known that physiologically relevant salt concentrations alter the affinity and dynamics for certain CB[7]-guest pairs arising from competition of cations binding at the CB[7] portal.^{21,22} Accordingly, the more dynamic behavior observed here for Xyl hydrogels in PBS is likely attributable to competition from a higher concentration of dissolved ions along with a reduced Debye length altering the electrostatic stabilizing forces for CB[7] in complex with the protonated primary and secondary amino groups of the Xyl guest. As neither the current or prior studies observed a crossover for the Ada hydrogel, it is not possible to determine from the frequency sweep if Ada hydrogel network dynamics are similarly impacted by the presence of salt, though the lack of protonating sites on

the Ada guest may indeed render it more resistant to elevated salt concentration.

Network Thermodynamics. With Xyl and Ada hydrogels prepared and validated using rheology to span the range of dynamic to quasi-static states, the thermodynamics of hydrogel network bonding were next evaluated according to principles of Transition State Theory.²³ Rheological stress relaxation experiments across a range of temperatures further emphasized the differences in bulk material dynamics arising from tunable crosslink affinity (Fig 1C-1D). By this method, Xyl hydrogels exhibited an exponential profile of stress relaxation (τ_R at $G(t)/G_0 = e^{-1}$) on the scale of seconds compared to a scale of hours for the less dynamic Ada hydrogels. Experiments for Ada hydrogels were truncated due to the long timescale required to observe the full exponential decay and confounding solvent evaporation entailed therein. Stress relaxation from these temperature-dependent studies can be evaluated with respect to temperature

using Eyring analysis in order to quantify thermodynamic properties that dictate the process of exchanging from a bound to a transition complex (ΔG^{\ddagger}) (Fig 1E-F). A comparison of these thermodynamic properties enables differences between Xyl and Ada to be clearly observed (Fig 1G). In particular, these results describe a significantly larger energy barrier for disassembly of the host-guest complexes in Ada hydrogels (ΔG^{\ddagger} = 99.6 kJ/mol) compared to the same transition for Xyl hydrogels (71.2 kJ/mol). Eyring analysis further informs the relative enthalpic and entropic contributions of this energy barrier. Notably, Xyl offered a more favorable enthalpy of CB[7] binding compared to Ada, anticipated due to electrostatic association between the protonated Xyl amines and the electronegative carbonyl portals of CB[7] that stabilize their complexation.^{24–26} The increased energy barrier for Ada crosslink reorganization instead arises from primarily entropic effects, in which the more hydrophobic adamantanol moiety is expected to have favorable binding entropy due to hydrating water

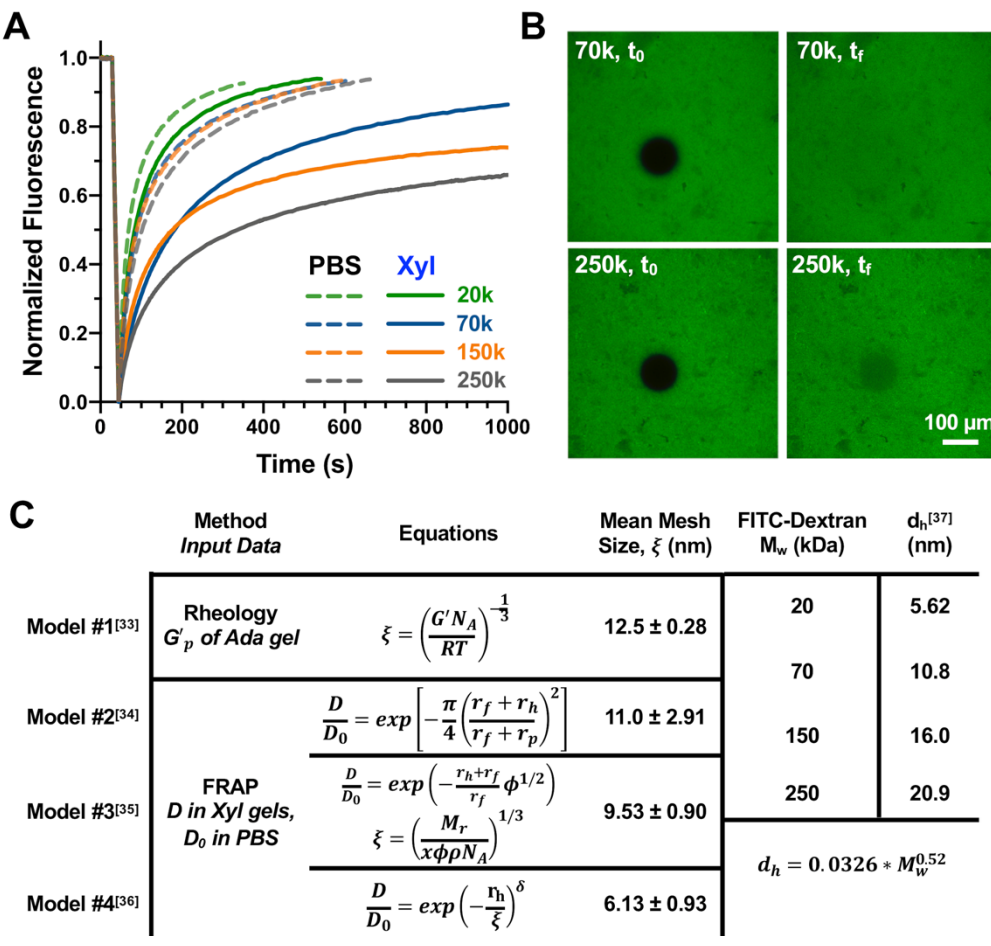


Figure 2. (a) Fluorescence recovery after photobleaching (FRAP) data for normalized ROI fluorescence of free (PBS) vs. Xylencapsulated FITC-dextran probes, showing an average of 3 experiments per trace. (b) Select representative images of hydrogels immediately following photobleaching, t₀, and at the study endpoint, t_f, with the scale bar shown applicable to all images. (c) Table displaying (*left*) applicable models of calculating mean mesh size of the hydrogel and (*right*) calculated hydrodynamic diameters of FITC-dextran macromolecule solutes. Models adapted according to references listed in superscript (refs ^{33–37}).

molecules being released into bulk solvent upon complexation, while the more hydrophilic Xyl pays some entropic penalty during the process of binding CB[7].^{12,27} Favorable Ada binding may also arise from restricted dissociation kinetics, theorized to result from the steric bulk of adamantane deforming the slightly narrower CB[7] portals.^{14,17,28,29} Ultimately, these results support the extension of underlying binding affinity and dynamics for CB[7]–guest motifs to the thermodynamics of crosslinking in supramolecular hydrogels. Specifically, these results indicate that Ada hydrogel crosslinking is not only less dynamic, but that this motif is subject to a larger thermodynamic, and specifically entropic, driving force favoring complexation.

Macromolecular Solute Diffusion. To explore the effect of dynamic crosslinking on diffusion of macromolecular solutes within these supramolecular hydrogels, a series of dilute FITC-dextran probes of different molecular weight (20, 70, 150, and 250 kDa) were encapsulated within Xyl hydrogels. The Xyl hydrogels were again prepared at 5 wt% in PBS with 1:1 stoichiometry between CB[7] and Xyl moieties. After equilibrating at room temperature, diffusion of fluorescent macromolecular solutes characterized using fluorescence recovery photobleaching (FRAP).30 Within the fluorescent field of view, a circular region of interest (ROI) was photobleached. The recovery of fluorescence within the ROI arises both from diffusion of photobleached probes out of the ROI and diffusion of fluorescently active probes into the ROI. This recovery in fluorescence signal within the ROI over time was quantified by image analysis (Fig 2A-2B). The recovery of fluorescence can then be used to calculate the rate of diffusion (D_r) by the simplified model:

$$D_r = 0.224 \, \frac{r^2}{\tau_{1/2}} \tag{2}$$

where r is the radius of the photobleached ROI and T1/2 is the characteristic time to 50% recovery of initial ROI fluorescence intensity.³¹ Rates of diffusion for FITC-dextran macromolecules dissolved in PBS are inversely related to the molecular weight of the probes, in agreement with the Stokes-Einstein model that predicts larger solutes to diffuse more slowly in solution.³² When encapsulated within Xyl hydrogels, FITC-dextran probes diffused more slowly than in free solution across all molecular weights, with larger molecular weight probes experiencing larger relative reductions in their diffusion rates (*Fig 2A*). For

instance, the diffusion of the Xyl-encapsulated 20 kDa probe (D_r = 15.6 $\mu m^2/s$) compared to the free 20 kDa probe (D_r = 25.3 $\mu m^2/s$) supported a ~38% reduction in the rate of diffusion (D/D_0 = 0.62). Meanwhile, the same comparison for the Xyl-encapsulated 250 kDa probe (D_r = 2.1 $\mu m^2/s$) compared to the free probe (D_r = 10.8 $\mu m^2/s$) resulted in a ~81% reduction in the rate of diffusion (D/D_0 = 0.19).

The mesh size (ξ) of the hydrogels was hypothesized to dictate size-dependent differences in the diffusion of encapsulated macromolecular solutes. In order to estimate mean ξ values for these materials, a number of models were used based on both rheological and FRAP results (*Fig. 2C*). 33–37 The mean ξ of both Xyl and Ada ideal network hydrogels are expected to be roughly identical in the fully bound conformation as a consequence of conserved topology of their PEG macromer building blocks. Differences in the estimated ξ values do arise based on the underlying assumptions of the mathematical models used. The rheology-based calculation (Model #1), derived from covalent ideal networks, was applied to the Ada hydrogel data given its demonstration of frequencyindependent G' behavior and a robust plateau modulus, yielding a mean mesh size of ξ_1 = 12.5 ± 0.28 nm. However, as this model was developed for covalently crosslinked hydrogels it may be expected to overestimate ξ for a dynamically crosslinked material as not all bonds are maximally formed at any given instance in time. Rheology-based pore size estimation was not applied to the Xyl hydrogels as the plateau region for G' remained outside the experimental frequency range. Instead, various FRAP-based models were applied to data for FITC-dextran encapsulated within Xyl hydrogels, yielding mean mesh size estimates of $\xi_2 = 11.0 \pm 2.91$ nm, $\xi_3 = 9.53 \pm 0.90$ nm, and ξ_4 = 6.13 ± 0.93 nm, with subscripts denoting the particular model used (Fig 2C). Of these FRAP-based models, differences in underlying assumptions account for the variation in estimated pore diameters. Notably, Model #2 arises from an Obstruction Model, relating probe diffusivity to relative sizes of solvated PEG fibers, fluorescent probes, and network pores, yet has reduced accuracy as solutes become significantly smaller than the mean mesh size.34 Model #3 incorporates all of these relationships while also considering macromer molecular weight, connectivity, bulk density, and polymer volume fraction.35 Unfortunately, polymer volume fraction determination often relies on gel swelling experiments that remain challenging for supramolecular materials

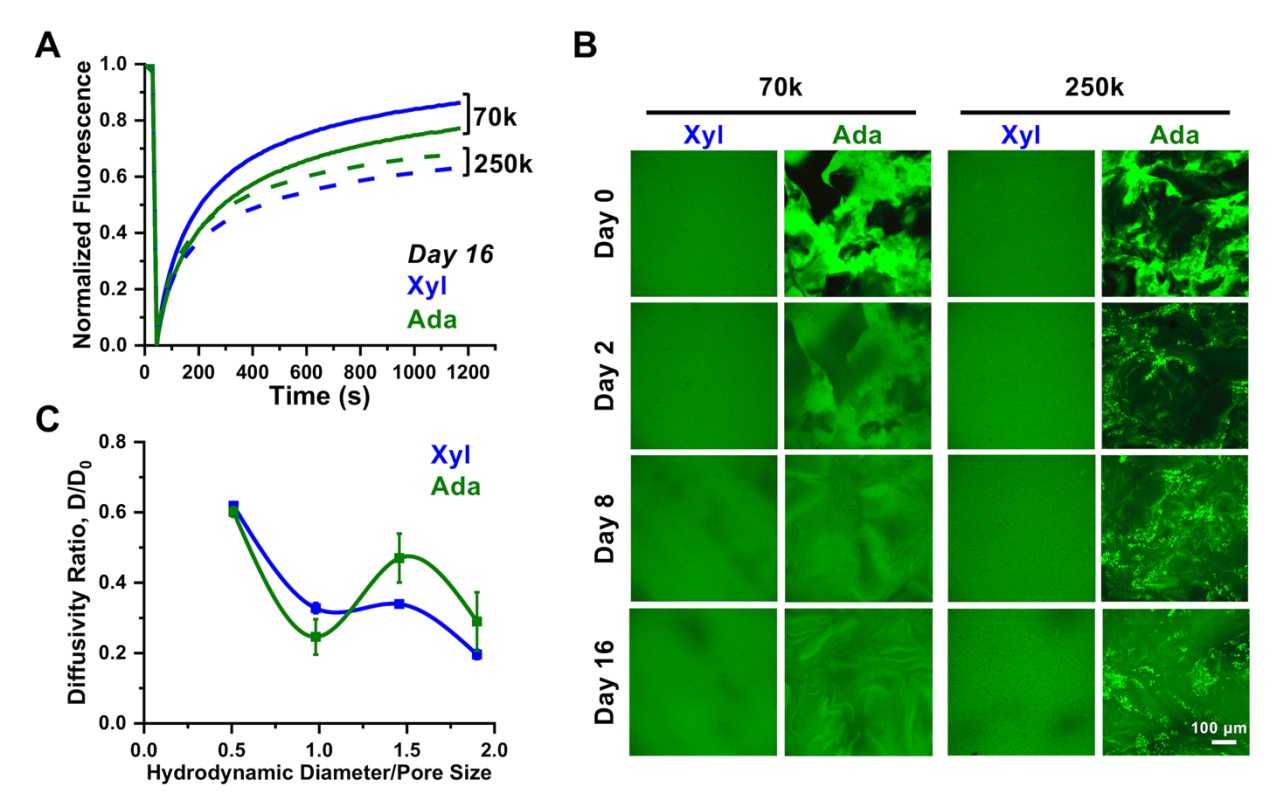


Figure 3. (a) Fluorescence recovery after photobleaching (FRAP) data averages (n=3) after 16 d equilibration for the 70 and 250 kDa probe encapsulated in Xyl and Ada hydrogels. (b) Select representative images displaying time-dependent hydrogel equilibration with aggregation of high molecular weight solutes by Ada hydrogel networks. (c) Analysis of diffusivity ratio versus the solute hydrodynamic diameter scaled to network pore size, exhibiting local maxima in the diffusivity ratio for solutes with dimensions in excess of the pore size.

vulnerable to erosion under bulk dilution. Model #4 is the only model originally derived for a supramolecular system, but a system with a markedly larger pore size and operating on a potentially distinct scale.³⁶ Viewed holistically, Model #2 is likely the most relevant estimate of our specific system, though as with the rheology model may also constitute a slight overestimate given dynamically associating network crosslinks.

Next, the hydrodynamic diameters (d_h) of FITC-dextran probes were calculated using a model optimized to fit the size of various molecular weight dextrans used in a variety of previous reports (*Fig. 2C*).³⁷ Comparing estimated pore sizes to the calculated hydrodynamic diameters (d_h) of the FITC-dextran probes used here supports the selection of these macromolecule solutes to span an appropriate range, wherein some solutes can traverse through the mean ξ of the hydrogel (*i.e.*, 20 and 70 kDa) while other solutes are too large to freely diffuse through the hydrogel porosity (*i.e.*, 150 and 250 kDa).

Diffusion In Different Dynamic States. Macromolecular size-dependent differences, wherein

some solutes readily diffuse within the hydrogel pore while larger solutes are effectively excluded from traversing the porosity, was next explored for comparison between dynamic Xyl hydrogels and quasi-static Ada hydrogels. For solutes sized near or above estimates for ξ , transport through the hydrogel was expected to occur concomitant with dynamic bond exchange due to steric limitations in passive transport through the hydrogel porosity. With the decreased dynamics of crosslinking, the Ada hydrogel would thus be expected to reduce solute transport relative to the more dynamic Xyl hydrogel given more frequent exchange of bonds in this more dynamic network. However, FRAP studies yielded somewhat surprising results (Fig 3A). For example, the 70 kDa probe conformed to preliminary expectations for the dependence on network dynamics, with diffusion and fluorescence recovery occurring more rapidly in Xyl hydrogels. Interestingly, the opposite trend was observed for the larger 250 kDa probe, which instead had more rapid diffusion and recovery observed in the more slowly dynamic Ada hydrogels. The impact of probe size on transport in dynamic versus quasi-static networks held for the 20 kDa and 150 kDa probes as well (Fig S2). In sum, the expected dynamic-dependent

trend of a higher solute diffusion rate in the more dynamic network was observed for the smaller solutes with d_h near (70 kDa) or below (20 kDa) the estimated ξ of these ideal networks. However, this trend was inverted for the larger solutes (150 and 250 kDa) with d_h in excess of the estimated ξ dimensions of the networks.

Results from FRAP studies on larger probes were initially somewhat surprising. Yet, these trends in solute diffusion, wherein smaller solutes exhibited faster diffusion in the more dynamic Xyl hydrogels while larger solutes diffused faster in the less dynamic Ada hydrogels, were supported by further unexpected observations made in confocal imaging over the course of gel equilibration leading up to FRAP studies (Fig 3B, Fig S3-S5). The more dynamic Xyl hydrogels equilibrated rapidly into a homogenous field of fluorescence upon encapsulation of all tested probes. However, the encapsulation of these same fluorescent probes within the Ada hydrogel resulted in highly heterogeneous mixing initially, likely arising from challenges in interfacial mixing between CB[7] and Ada macromers due to high-affinity, slowly dynamic crosslinking. Kinetically limited macromer mixing may introduce interfacial transport limitations and/or regions of heterogeneous network architecture to confound FRAP measurements. Accordingly, 16 days of network equilibration was allowed before comparative FRAP experiments between the Xyl and Ada networks. Over this time, the smaller macromolecular solutes capable of fitting within a single hydrogel pore (20 and 70 kDa) equilibrated with the network to yield a homogenous fluorescent field, supporting the 16 day timeline for macromer network equilibration used. Yet, solutes estimated to be too large to fit within a single hydrogel pore (150 and 250 kDa) instead formed punctate fluorescent clusters in the Ada hydrogel over this same 16 day equilibration, yielding a fluorescent field containing aggregates of fluorescent probe molecules.

This observation of punctate structures supports a phenomenon of solute network exclusion, which we hypothesize to result from the increased thermodynamic driving forces favoring an ideal network in the case of high-affinity Ada crosslinking. Reminiscent of the hydrophobic effect that drives the aggregation of hydrocarbons in an environment to minimize system free energy by maximizing solvent entropy, here it is postulated that the higher thermodynamic driving

crosslinking in the Ada hydrogel effectively maximizes ideal network bonding by sequestering network-disrupting larger solutes into aggregates. This phenomenon, arising from high-affinity crosslink chemistry driving ideal network formation, stands in contrast to reports of controlled solute diffusion arising from polymer hydrogel architectures designed from building blocks that phase separate and give rise to microchannels.³⁸⁻⁴¹ As the Ada network equilibrates, the high entropic favorability of complex formation acts to structure network-disrupting solutes into aggregates and minimize the number network bonds sacrificed, resulting in the larger fluorescent probes forming punctate aggregates rather than homogenous field over 16 days of network equilibration. This hypothesis is supported by observation of homogenous fields for all probes in the lower affinity Xyl hydrogels that do not have the same entropic driving force for crosslink formation, as well as homogenous fields in Ada hydrogels when encapsulating smaller solutes (20 and 70 kDa) that can be accommodated within the mean ξ dimensions of these networks. Moreover, data from both Xyl hydrogels and free probes indicated that this phenomenon does not arise from an aggregated state of larger solutes either initially or forming over time (Fig S3-S4). The exclusion phenomenon for larger solutes, therefore, is postulated to create tortuous channels through which solutes traverse the Ada network without need for bond exchange, thus leading to faster diffusion compared to the more dynamic Xyl hydrogels. Though the presence of networkdisrupting solutes would reduce hydrogel mechanical properties above some critical threshold concentration, the inclusion of dextran here at only 1.2% by mass relative to the macromer does not yield appreciable changes to the network that could be quantified by rheology.

When plotting diffusivity of macromolecular solutes as its ratio between the hydrogel and free solution (D/D₀) versus the solute hydrodynamic diameter (d_h) divided by ξ , the data notably diverged from the Stokes-Einstein and Obstruction Theory predictions of a steady decrease in diffusivity as d_h approached ξ (*Fig* 3C). Instead, the data included unexpected local maxima in the midst of the otherwise expected decreasing trend, evident in the Xyl hydrogels and more pronounced in the less dynamic Ada hydrogels; in both cases local maxima arise as d_h surpasses ξ . These experimental findings support the local maxima predicted from the recently reported Multiscale

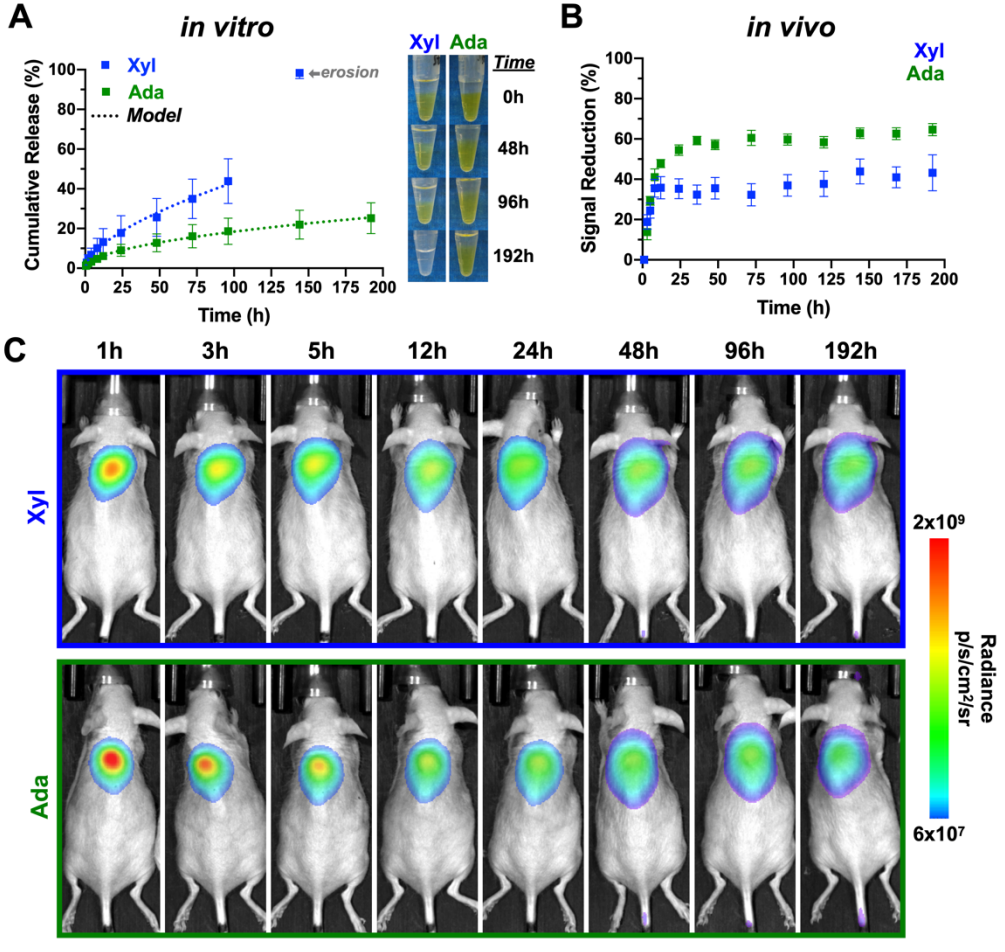


Figure 4. (a) Bulk release studies of a 70 kDa FITC-dextran probe from hydrogels *in vitro* (n=3 gels/group); data reproduced with permission (ref ¹⁸). (b) *In vivo* release of 70 kDa Cy5-dextran solute from subcutaneously injected hydrogels, quantified as the percent reduction in signal at the depot site using *in vivo* imaging (n=5 mice/group). (c) Representative *in vivo* fluorescent images of Cy5-dextran solute encapsulated within subcutaneous Xyl and Ada hydrogels, overlaid onto mouse photographs.

Diffusion Model (MSDM).4 This newly developed model works to unify Free Volume Theory, which assumes solutes far smaller than pore size, and Obstruction Theory, which assumes solutes similarly sized or larger than pores. By appropriately weighing competing diffusion mechanisms across distinct length scales within a single model, previously unexpected diffusion phenomena can be described. Though the data collected for the Xyl and Ada hydrogels exhibit the same phenomenon predicted by the MSDM model, these do not readily overlay with the curves of this model due to the inherent differences between the covalent networks used to develop the model and the dynamic hydrogels studied herein. Namely, in these dynamic systems probes in excess of ξ have much greater mobility than in covalent gels, leading to a phase mismatch when applying the MSDM model parameters to the present data. For instance, probes far in excess of ξ can still diffuse within dynamic hydrogels through crosslink bond exchange, or by diffusing along with the macromers

comprising the network, whereas such solutes would be effectively trapped in a covalent network. However, the general behavior predicted by the MSDM model of local maxima in relative diffusion rates at an intermediate solute size was conserved in the experimental data gathered here.

Controlled Release of Macromolecules. The relevance of delivering macromolecular therapies using hydrogels also inspires interest in understanding how these networks, with disparate dynamics, translate to the controlled release of encapsulated molecules *in vitro* and *in vivo*. For these studies, the 70 kDa probe was chosen to be near the dimension of ξ and also as it exhibited positively correlated dynamics-dependent differences in diffusion between the Xyl and Ada networks in FRAP studies. According to previous studies on this 70 kDa dextran probe, 18 release from hydrogels into a bulk solution was correlated with dynamics, in alignment with preliminary expectations (*Fig 4A*). When fitting these data to the Korsmeyer-

Peppas model in which fractional solute release from a hydrogel is related to the product of a kinetic constant and release time, $M_t/M_\infty = kt^n$, 6 Xyl hydrogels exhibited characteristics of anomalous and erosion-dominated release; this is supported by complete gel erosion at 6 d under conditions of bulk dilution. The Ada hydrogels, meanwhile, demonstrated release more consistent with Fickian diffusion according to the Korsmeyer-Peppas model. These data corroborate data from FRAP for faster release in the more dynamic Xyl system, though the introduction of network swelling and erosion of Xyl hydrogels in the setting of a bulk solvent suggests release is governed by additional mechanisms beyond solely diffusion.

In an effort to correlate macromolecular release in vitro with in vivo function, hydrogels encapsulating Cy5labeled 70 kDa dextran were injected subcutaneously in mice and monitored using live animal in vivo imaging. Both Xyl and Ada hydrogels demonstrated rapid initial burst release, evidenced by signal reduction over the first ~8 h following injection (Fig. 4B-C). Beyond this point, these two materials diverged, as release from the Xyl hydrogels stalled while Ada hydrogels continued to release for ~36 h before also plateauing. Interestingly, this comparative release behavior was opposite to that predicted by release experiments in vitro. Specifically, the initial burst and subsequent plateau in release with a large fraction of dye retained in the hydrogel, observed for both hydrogels, was unexpected. It is conceivable that the initial burst happens as a result of material deformation upon injection as well as expulsion of some water and smaller molecular weight dye-linked solutes from the hydrogel under compression of the skin. This is an outcome deserving of further exploration given burst release from a hydrogel upon injection may interfere with many applications centered on controlled therapeutic release. In regards to the apparent plateau in release, it was demonstrated previously that these hydrogels do not elicit formation of a fibrotic capsule to act as a transport barrier, 18 nor would such a capsule be expected to form within hours to days of injection. Instead, it is postulated that accumulation of cells and proteins tissue/material interface may halt release from the networks, with this process being accelerated in hydrogels composed of the charge-bearing Xyl guest compared to that in networks prepared from the neutral Ada guest. The increased adsorption of serum proteins has been reported for other classes of positively charged hydrogels,42 though further exploration of these phenomena is warranted here. Indeed, histological analysis performed at the endpoint of these studies demonstrated the presence of a layer of infiltrating cells at the tissue/material interface for both hydrogels, with the apparent thickness of this layer being larger in Xyl versus Ada hydrogels (Fig S6). This discrepancy in release behavior from in vitro to in vivo models therefore highlights a key challenge in predicting controlled release characteristics of dynamic supramolecular networks through subjecting these to bulk dilution in vitro. Though Xyl hydrogels exhibited dissolution and erosion within 6 d in a standard bulk release set-up, the same hydrogels remained intact and could be retrieved from subcutaneous tissue through necropsy at 9 d with no apparent reduction in hydrogel volume compared to Ada hydrogels. Moreover, in spite of more rapid probe diffusion demonstrated in FRAP studies and more rapid release in vitro, the in vivo release from Xvl materials was effectively halted within hours. As such, care must be taken when developing supramolecular hydrogel platforms for controlled release macromolecules to carefully correlate in vitro release assays with in vivo performance.

CONCLUSIONS

In this work, two hydrogels of differing crosslink dynamics were investigated to study the impact of this design parameter on the internal diffusion and bulk release of macromolecular solutes. By tuning crosslink thermodynamics and resultant kinetics to span dynamic to quasi-static states using high-affinity CB[7]-guest complex crosslinking, the propagation of tunable complex affinities was manifest in bulk material properties. Eyring analysis performed on temperature-dependent stress relaxation data enabled the thermodynamics of these crosslinks to be characterized, offering evidence for thermodynamic driving forces favoring a more stable ideal network in the higher affinity Ada hydrogel. These differences in crosslink thermodynamics resulted in surprising the diffusion differences in behavior macromolecular solutes within these hydrogels. FRAP studies revealed the expected dynamics-dependent differences in diffusion for smaller solutes near or below the estimated ξ dimensions, with faster transport in the Xyl hydrogel than in the less dynamic Ada hydrogel. However, macromolecular solutes with hydrodynamic diameters exceeding ξ exhibited nonclassical diffusion behavior, an effect accentuated in the Ada hydrogels with a much

thermodynamic driving force favoring an idealized network. This phenomenon corresponded to an observation of solute aggregation and network exclusion, wherein macromolecular solutes incapable of encapsulation within a single network pore were afforded channels to diffuse through the network, thereby circumventing predictions for crosslink dissociation-dependent diffusion behavior. Toward translational use of these materials, bulk release of 70 kDa dextran was assessed both in vitro and in vivo. The in vitro release data was primarily consistent with expectations from FRAP studies, as a macromolecular solute capable of encapsulation within the network porosity exhibited release rates corresponding to network dynamics, though augmented by network swelling and erosion under conditions of dilution. However, release in vivo exhibited an inverse relationship, with the less dynamic Ada hydrogel releasing more of the encapsulated fluorescent probe during the initial 36 h before both Xyl and Ada release profiles plateaued for a period of 7 d. This seeming discrepancy between in vitro and in vivo release behavior underscores the importance of further investigation into both the fundamental material science and thermodynamics alongside biomedical applications of supramolecular hydrogel networks.

EXPERIMENTAL SECTION

Macromer Synthesis. CB[7]-PEG_{8a}, Xyl-PEG_{8a}, and Ada-PEG_{8a} were synthesized and fully characterized, as previously reported.¹⁸

Rheology. Oscillatory rheology was performed on a TA Instruments Discovery HR-2 rheometer. A 20 mm, 2° conical upper geometry was used for all experiments. The Peltier stage was fitted with a solvent trap to minimize evaporation from samples during testing. Following amplitude strain sweeps at 10 rad/s from 0.1 to 200% strain, frequency sweeps were conducted at 2% strain from 0.1 to 200 rad/s on Xyl and Ada gels; this strain was verified to be in the linear viscoelastic region for all samples. Stress relaxations experiments were then performed on 5 wt% Xyl and Ada gels and included a temperature equilibration followed by the application of a constant 2% strain at various temperatures. The Xyl gel was equilibrated for 3 min at temperatures ranging from 5-25°C and strained for 1000 s. The Ada gel was equilibrated for 10 min at temperatures between 25-45°C and strained for up to 10000 s.

FRAP. Fluorescence recovery after photobleaching (FRAP) was performed based on a previously published procedure.30 Briefly, a Nikon A1R inverted confocal microscope equipped with a 20X objective lens (N.A. 0.75) was used. Gel samples were pre-mixed within a syringe and loaded into a hybridization chamber (Electron Microscopy Sciences, 70333-42). Imaging was performed 30 µm above the gel/coverslip interface with the detector voltage adjusted so that the median fluorescence was approximately 2000 intensity units. Three positions across the center of the well were acquired for each gel condition. Two circular regions of interest (ROI) with diameters of 105 µm each were monitored in the field of view; one ROI was designated for active photobleaching with the other as a control for passive bleaching during imaging. Photobleaching was performed using 405 nm, 488 nm, 561 nm, and 638 nm laser light at a power setting of 100% to achieve at least 75% decrease in signal intensity. Each ROI was imaged every 2 s for 30 s, photobleached for 14 s, imaged every 2 s for 135 s, and imaged every 10 s for 990 s. Intensity analysis was done using Nikon Elements software (v. 5.20.02).

Release Studies. In vitro release experiments were conducted as previously reported.18 For studies in vivo, a previously reported Cy5-labeled fluorescent dextran was substituted in order to enable better visualization and signal quantification via imaging.43 Hairless 8-wk old male SKH1-E mice (Charles River) were injected with 80 µL hydrogels prepared by mixing CB[7]-PEG8a with equimolar amount of Xyl-PEG8a or Ada-PEG8a at a total macromer concentration of 5 wt%. Hydrogels also included 0.6 mg/ml of Cy5-labeled 70 kDa Dextran. Mice were briefly anesthetized with inhaled isoflurane to enable precise localization of injection. Subsequently, these mice were serially imaged using an AMI HT in vivo imager (Spectral Instruments) at the noted timepoints. Studies were conducted with n=5 mice per group. Data were analyzed and quantified using the Aura software package included with the imager. Following 8 d of imaging, mice were euthanized on day 9 and the hydrogel and surrounding tissue were assessed by gross necropsy to hydrogel verify retention and characterize inflammation. The gel and surrounding tissue was fixed in formalin, and subjected to routine histological processing, sectioning, and staining with H&E. All experiments followed a protocol approved by the University of Notre Dame Animal Care and Use Committee (IACUC) and adhered to all relevant Institutional, State, and Federal guidelines.

ASSOCIATED CONTENT

Supporting Information

The Supporting Information is available free of charge on the ACS Publications website.

Supplemental FRAP Data (.PDF)

AUTHOR INFORMATION

Corresponding Author

* mwebber@nd.edu

Notes

The authors declare no competing financial interests.

ACKNOWLEDGMENT

MJW gratefully acknowledges funding support from the National Institutes of Health (R35GM137987), the National Science Foundation (BMAT, 1944875), a 3M Non-Tenured Faculty Award (3M Company), and the University of Notre Dame "Advancing our Vision" initiative. Imaging was performed in the Optical Microscopy and In Vivo Imaging cores of the Notre Dame Integrated Imaging Facility. Rheology was performed in the ND Energy Materials Characterization Facility. Schematics were created using BioRender.com.

REFERENCES

- (1) Li, J.; Mooney, D. J. Designing Hydrogels for Controlled Drug Delivery. *Nat Rev Mater* **2016**, *1* (12). https://doi.org/10.1038/natrevmats.2016.71.
- (2) Correa, S.; Grosskopf, A. K.; Lopez Hernandez, H.; Chan, D.; Yu, A. C.; Stapleton, L. M.; Appel, E. A. Translational Applications of Hydrogels. *Chem. Rev.* **2021**, *121* (18), 11385–11457.
- (3) Peppas, N. A.; Hilt, J. Z.; Khademhosseini, A.; Langer, R. Hydrogels in Biology and Medicine: From Molecular Principles to Bionanotechnology. *Advanced Materials*. 2006, pp 1345–1360. https://doi.org/10.1002/adma.200501612.
- (4) Axpe, E.; Chan, D.; Offeddu, G. S.; Chang, Y.; Merida, D.; Hernandez, H. L.; Appel, E. A. A Multiscale Model for Solute Diffusion in Hydrogels. *Macromolecules* 2019, 52 (18), 6889–6897.
- (5) Peppas, N. A.; Narasimhan, B. Mathematical Models in Drug Delivery: How Modeling Has Shaped the Way We Design New Drug Delivery Systems. J. Control. Release 2014, 190, 75–81.
- (6) Korsmeyer, R. W.; Gurny, R.; Doelker, E.; Buri, P.; Peppas, N. A. Mechanisms of Solute Release from Porous Hydrophilic Polymers. *International Journal of Pharmaceutics*. 1983, pp 25–35. https://doi.org/10.1016/0378-5173(83)90064-9.
- (7) Webber, M. J.; Appel, E. A.; Meijer, E. W.; Langer, R. Supramolecular Biomaterials. *Nat. Mater.* **2016**, *15* (1), 13–26.

- (8) Webber, M. J.; Langer, R. Drug Delivery by Supramolecular Design. *Chem. Soc. Rev.* **2017**, *46* (21), 6600–6620.
- (9) Mantooth, S. M.; Munoz-Robles, B. G.; Webber, M. J. Dynamic Hydrogels from Host-Guest Supramolecular Interactions. *Macromol. Biosci.* 2019, 19 (1), e1800281.
- (10) Rodell, C. B.; Kaminski, A. L.; Burdick, J. A. Rational Design of Network Properties in Guest-Host Assembled and Shear-Thinning Hyaluronic Acid Hydrogels. *Biomacromolecules* **2013**, *14* (11), 4125–4134.
- (11) Appel, E. A.; del Barrio, J.; Loh, X. J.; Scherman, O. A. Supramolecular Polymeric Hydrogels. *Chem. Soc. Rev.* **2012**, *41* (18), 6195–6214.
- (12) Braegelman, A. S.; Webber, M. J. Integrating Stimuli-Responsive Properties in Host-Guest Supramolecular Drug Delivery Systems. *Theranostics* 2019, 9 (11), 3017–3040.
- (13) Sahoo, J. K.; VandenBerg, M. A.; Webber, M. J. Injectable Network Biomaterials via Molecular or Colloidal Self-Assembly. Adv. Drug Deliv. Rev. 2018, 127, 185–207.
- (14) Barrow, S. J.; Kasera, S.; Rowland, M. J.; del Barrio, J.; Scherman, O. A. Cucurbituril-Based Molecular Recognition. *Chemical Reviews*. 2015, pp 12320–12406. https://doi.org/10.1021/acs.chemrev.5b00341.
- (15) Kim, J.; Jung, I.-S.; Kim, S.-Y.; Lee, E.; Kang, J.-K.; Sakamoto, S.; Yamaguchi, K.; Kim, K. New Cucurbituril Homologues: Syntheses, Isolation, Characterization, and X-Ray Crystal Structures of Cucurbit[n]uril (n = 5, 7, and 8). *J. Am. Chem. Soc.* **2000**, *122* (3), 540–541.
- (16) Zou, L.; Braegelman, A. S.; Webber, M. J. Spatially Defined Drug Targeting by in Situ Host-Guest Chemistry in a Living Animal. ACS Central Science. 2019, pp 1035–1043. https://doi.org/10.1021/acscentsci.9b00195.
- (17) Cao, L.; Śekutor, M.; Zavalij, P. Y.; Mlinarić-Majerski, K.; Glaser, R.; Isaacs, L. Cucurbit[7]uril·guest Pair with an Attomolar Dissociation Constant. *Angew. Chem. Int. Ed Engl.* **2014**, *53* (4), 988–993.
- (18) Zou, L.; Braegelman, A. S.; Webber, M. J. Dynamic Supramolecular Hydrogels Spanning an Unprecedented Range of Host-Guest Affinity. *ACS Appl. Mater. Interfaces* **2019**, *11* (6), 5695–5700.
- (19) Maikawa, C. L.; d'Aquino, A. I.; Vuong, E. T.; Su, B.; Zou, L.; Chen, P. C.; Nguyen, L. T.; Autzen, A. A. A.; Mann, J. L.; Webber, M. J.; Appel, E. A. Affinity-Directed Dynamics of Host-Guest Motifs for Pharmacokinetic Modulation Supramolecular PEGylation. Biomacromolecules 2021, 22 (8), 3565–3573.
- (20) Webber, M. J.; Tibbitt, M. W. Dynamic and Reconfigurable Materials from Reversible Network Interactions. *Nature Reviews Materials*. 2022. https://doi.org/10.1038/s41578-021-00412-x.
- (21) Hu, C.; Grimm, L.; Prabodh, A.; Baksi, A.; Siennicka, A.; Levkin, P. A.; Kappes, M. M.; Biedermann, F. Covalent cucurbit[7]uril–dye Conjugates for Sensing in Aqueous Saline Media and Biofluids. *Chemical Science*. 2020, pp 11142–11153. https://doi.org/10.1039/d0sc03079a.
- (22) Tang, H.; Fuentealba, D.; Ko, Y. H.; Selvapalam, N.; Kim,

- K.; Bohne, C. Guest Binding Dynamics with cucurbit[7]uril in the Presence of Cations. *J. Am. Chem. Soc.* **2011**, *133* (50), 20623–20633.
- (23) Marco-Dufort, B.; Iten, R.; Tibbitt, M. W. Linking Molecular Behavior to Macroscopic Properties in Ideal Dynamic Covalent Networks. *J. Am. Chem. Soc.* **2020**, *142* (36), 15371–15385.
- (24) Jeon, W. S.; Moon, K.; Park, S. H.; Chun, H.; Ko, Y. H.; Lee, J. Y.; Lee, E. S.; Samal, S.; Selvapalam, N.; Rekharsky, M. V.; Sindelar, V.; Sobransingh, D.; Inoue, Y.; Kaifer, A. E.; Kim, K. Complexation of Ferrocene Derivatives by the cucurbit[7]uril Host: A Comparative Study of the Cucurbituril and Cyclodextrin Host Families. J. Am. Chem. Soc. 2005, 127 (37), 12984–12989.
- (25) Rekharsky, M. V.; Mori, T.; Yang, C.; Ko, Y. H.; Selvapalam, N.; Kim, H.; Sobransingh, D.; Kaifer, A. E.; Liu, S.; Isaacs, L.; Chen, W.; Moghaddam, S.; Gilson, M. K.; Kim, K.; Inoue, Y. A Synthetic Host-Guest System Achieves Avidin-Biotin Affinity by Overcoming Enthalpy-Entropy Compensation. *Proc. Natl. Acad. Sci.* U. S. A. 2007, 104 (52), 20737–20742.
- (26) Shetty, D.; Khedkar, J. K.; Park, K. M.; Kim, K. Can We Beat the Biotin-Avidin Pair?: cucurbit[7]uril-Based Ultrahigh Affinity Host-Guest Complexes and Their Applications. *Chem. Soc. Rev.* **2015**, 44 (23), 8747–8761.
- (27) Moghaddam, S.; Yang, C.; Rekharsky, M.; Ko, Y. H.; Kim, K.; Inoue, Y.; Gilson, M. K. New Ultrahigh Affinity Host-Guest Complexes of cucurbit[7]uril with bicyclo[2.2.2]octane and Adamantane Guests: Thermodynamic Analysis and Evaluation of M2 Affinity Calculations. *J. Am. Chem. Soc.* **2011**, *133* (10), 3570–3581.
- (28) Jiménez-Cruz, F.; García-Gutiérrez, J. L. Molecular Size and Shape Properties of Diamondoid Molecules Occurring in Crude Oil. *Arabian Journal of Chemistry*. 2020, pp 8592–8599. https://doi.org/10.1016/j.arabjc.2020.09.043.
- (29) Escobar, L.; Ballester, P. Molecular Recognition in Water Using Macrocyclic Synthetic Receptors. *Chem. Rev.* **2021**, 121 (4), 2445–2514.
- (30) Branco, M. C.; Pochan, D. J.; Wagner, N. J.; Schneider, J. P. Macromolecular Diffusion and Release from Self-Assembled Beta-Hairpin Peptide Hydrogels. *Biomaterials* 2009, 30 (7), 1339–1347.
- (31) Kang, M.; Day, C. A.; Kenworthy, A. K.; DiBenedetto, E. Simplified Equation to Extract Diffusion Coefficients from Confocal FRAP Data. *Traffic* **2012**, *13* (12), 1589–1600.
- (32) Jowkarderis, L.; van de Ven, T. G. M. Mesh Size Analysis of Cellulose Nanofibril Hydrogels Using Solute

- Exclusion and PFG-NMR Spectroscopy. *Soft Matter* **2015**, *11* (47), 9201–9210.
- (33) Karvinen, J.; Ihalainen, T. O.; Calejo, M. T.; Jönkkäri, I.; Kellomäki, M. Characterization of the Microstructure of Hydrazone Crosslinked Polysaccharide-Based Hydrogels through Rheological and Diffusion Studies. Mater. Sci. Eng. C Mater. Biol. Appl. 2019, 94, 1056–1066.
- (34) Amsden, B. An Obstruction-Scaling Model for Diffusion in Homogeneous Hydrogels. *Macromolecules* **1999**, 32 (3), 874–879.
- (35) Hagel, V.; Haraszti, T.; Boehm, H. Diffusion and Interaction in PEG-DA Hydrogels. *Biointerphases* **2013**, *8* (1), 36.
- (36) Wallace, M.; Adams, D. J.; Iggo, J. A. Analysis of the Mesh Size in a Supramolecular Hydrogel by PFG-NMR Spectroscopy. *Soft Matter* **2013**, *9* (22), 5483.
- (37) Hadjiev, N. A.; Amsden, B. G. An Assessment of the Ability of the Obstruction-Scaling Model to Estimate Solute Diffusion Coefficients in Hydrogels. *J. Control. Release* **2015**, 199, 10–16.
- (38) Cui, S.; Yu, L.; Ding, J. Semi-Bald Micelles and Corresponding Percolated Micelle Networks of Thermogels. *Macromolecules* **2018**, *51* (16), 6405–6420.
- (39) Xue, K.; Zhao, X.; Zhang, Z.; Qiu, B.; Tan, Q. S. W.; Ong, K. H.; Liu, Z.; Parikh, B. H.; Barathi, V. A.; Yu, W.; Wang, X.; Lingam, G.; Hunziker, W.; Su, X.; Loh, X. J. Sustained Delivery of Anti-VEGFs from Thermogel Depots Inhibits Angiogenesis without the Need for Multiple Injections. *Biomater Sci* **2019**, *7* (11), 4603–4614.
- (40) Censi, R.; Vermonden, T.; Deschout, H.; Braeckmans, K.; di Martino, P.; De Smedt, S. C.; van Nostrum, C. F.; Hennink, W. E. Photopolymerized Thermosensitive poly(HPMAlactate)-PEG-Based Hydrogels: Effect of Network Design on Mechanical Properties, Degradation, and Release Behavior. *Biomacromolecules* **2010**, *11* (8), 2143–2151.
- (41) Rodell, C. B.; Highley, C. B.; Chen, M. H.; Dusaj, N. N.; Wang, C.; Han, L.; Burdick, J. A. Evolution of Hierarchical Porous Structures in Supramolecular Guest-Host Hydrogels. *Soft Matter* **2016**, *12* (37), 7839–7847.
- (42) Yamada, Y.; Fichman, G.; Schneider, J. P. Serum Protein Adsorption Modulates the Toxicity of Highly Positively Charged Hydrogel Surfaces. *ACS Appl. Mater. Interfaces* **2021**, *13* (7), 8006–8014.
- (43) Zou, L.; Su, B.; Addonizio, C. J.; Pramudya, I.; Webber, M. J. Temperature-Responsive Supramolecular Hydrogels by Ternary Complex Formation with Subsequent Photo-Cross-Linking to Alter Network Dynamics. *Biomacromolecules* **2019**, 20 (12), 4512–4521.

